nature genetics

# Mutational landscape and clonal architecture in grade II and III gliomas

Hiromichi Suzuki[1,2,11], Kosuke Aoki[1,2,11], Kenichi Chiba[3], Yusuke Sato[2], Yusuke Shiozawa[2], Yuichi Shiraishi[3], Teppei Shimamura[4], Atsushi Niida[3], Kazuya Motomura[1], Fumiharu Ohka[1,5], Takashi Yamamoto[1], Kuniaki Tanahashi[1], Melissa Ranjit[1], Toshihiko Wakabayashi[1], Tetsuichi Yoshizato[2], Keisuke Kataoka[2], Kenichi Yoshida[2], Yasunobu Nagata[2], Aiko Sato-Otsubo[2], Hiroko Tanaka[3], Masashi Sanada[2], Yutaka Kondo[5], Hideo Nakamura[6], Masahiro Mizoguchi[7], Tatsuya Abe[8], Yoshihiro Muragaki[9], Reiko Watanabe[10], Ichiro Ito[10], Satoru Miyano[3], Atsushi Natsume[1,12] & Seishi Ogawa[2,12]

**Grade II and III gliomas are generally slowly progressing brain cancers, many of which eventually transform into more aggressive tumors. Despite recent findings of frequent mutations in *IDH1* and other genes, knowledge about their pathogenesis is still incomplete. Here, combining two large sets of high-throughput sequencing data, we delineate the entire picture of genetic alterations and affected pathways in these glioma types, with sensitive detection of driver genes. Grade II and III gliomas comprise three distinct subtypes characterized by discrete sets of mutations and distinct clinical behaviors. Mutations showed significant positive and negative correlations and a chronological hierarchy, as inferred from different allelic burdens among coexisting mutations, suggesting that there is functional interplay between the mutations that drive clonal selection. Extensive serial and multi-regional sampling analyses further supported this finding and also identified a high degree of temporal and spatial heterogeneity generated during tumor expansion and relapse, which is likely shaped by the complex but ordered processes of multiple clonal selection and evolutionary events.**



Gliomas represent approximately 80% of malignant brain tumors, with an age-adjusted mortality rate of 4.25/100,000 per year in the United States[1]. Although a number of distinct histological types are recognized under this category in the World Health Organization (WHO) classification system, gliomas are classified into four major histological grades, grades I–IV, according to their histopathology and clinical behavior[2,3]. Grade IV glioma, or glioblastoma (GBM), notoriously has a highly aggressive clinical course with a median survival time of only 12.2 to 18.2 months after diagnosis[4,5]. In contrast, accounting for approximately one-third of all gliomas, gliomas of lower grade are usually less aggressive tumors with a longer, indolent clinical course, suggesting that they have distinctive genetic features and molecular pathogenesis relative to grade IV gliomas[6–8]. However, despite their prolonged prognosis in recent years, many cases of grade II and III glioma, especially those having histology consistent with astrocytomas, oligodendrogliomas and oligoastrocytomas, eventually progress to a more aggressive tumor or GBM over years[3]. Thus, gliomas in these categories are thought to exemplify a typical model of multistep oncogenesis during which multiple rounds of acquisition of new mutations together with clonal selection and evolution take place to shape the establishment and progression of these gliomas. Thus, understanding the genetic sequences underlying this oncogenic process comprises an essential part of the knowledge that will be required to devise better management of this tumor type.

In this regard, recent studies have reported a unique genomic picture of grade II and III gliomas[9–11] that shows distinct molecular lesions from those typically found in GBMs. These tumors have an extremely high frequency of *IDH1* or *IDH2* mutation, which is accompanied either by 1p and 19q co-deletion and a mutated *TERT* promoter or by *TP53* mutations with or without *ATRX* mutations, together with other mutations such as those involving *CIC* and *FUBP1* (refs. 12–17). However, in the absence of large-scale, unbiased analysis, the full spectrum of genetic alterations in grade II and III gliomas and the role of these alterations in clonal evolution and tumor phenotypes are still unclear. In the current study, we performed an extensive genetic analysis by combining two independent sets of genomic data from large cohorts of grade II and III gliomas from Japan (JPN) and The Cancer Genome Atlas (TCGA) Consortium to delineate a complete

[1]Department of Neurosurgery, Nagoya University School of Medicine, Nagoya, Japan. [2]Department of Pathology and Tumor Biology, Kyoto University, Kyoto, Japan. [3]Human Genome Center, Institute of Medical Science, The University of Tokyo, Tokyo, Japan. [4]Division of Systems Biology, Nagoya University School of Medicine, Nagoya, Japan. [5]Department of Epigenomics, Nagoya City University Graduate School of Medical Sciences, Nagoya, Japan. [6]Department of Neurosurgery, Kumamoto University, Kumamoto, Japan. [7]Department of Neurosurgery, Graduate School of Medical Sciences, Kyushu University, Fukuoka, Japan. [8]Department of Neurosurgery, Oita University, Oita, Japan. [9]Department of Neurosurgery, Tokyo Women's Medical University, Tokyo, Japan. [10]Division of Clinical Pathology, Shizuoka Cancer Center, Shizuoka, Japan. [11]These authors contributed equally to this work. [12]These authors jointly supervised this work. Correspondence should be addressed to S.O. (sogawa-tky@umin.ac.jp) or A. Natsume (anatsume@med.nagoya-u.ac.jp).

Received 7 October 2014; accepted 13 March 2015; published online 13 April 2015; doi:10.1038/ng.3273

landscape of genetic lesions in these gliomas and also investigated the roles of the identified alterations in clonal evolution and tumor progression by employing sampling at multiple time points and from multiple tumor regions in 14 cases with grade II gliomas.

## RESULTS

### Whole-exome and targeted deep sequencing

To obtain a comprehensive registry of driver genes in grade II and III gliomas, we first performed whole-exome sequencing on paired tumor-normal DNA samples from 52 JPN patients with grade II and III gliomas (Online Methods). We also downloaded raw sequencing data from the whole-exome sequencing of 425 grade II and III glioma samples, which had been generated and made publically available by the TCGA Consortium. We uniformly analyzed the whole-exome sequencing data from the combined JPN and TCGA cohorts for somatic mutations using our in-house pipelines[18–20] (**Supplementary Fig. 1**). The mean coverage for JPN and TCGA cases was 130× and 94×, respectively. Excluding 11,718 events called in a single TCGA case (TCGA-DU-6392-01A), a total of 12,995 single-nucleotide variants (SNVs) and 1,116 insertions-deletions (indels) were called (**Supplementary Fig. 2** and **Supplementary Tables 1** and **2**), for which the true positive rates were estimated to be 97.8% and 96.7% on the basis of validation sequencing of 725 randomly selected SNVs and 61 randomly selected indels in JPN cases (Online Methods and **Supplementary Table 3**). The genome-wide mutation rate was almost identical for the JPN (0.77 mutations/Mb) and TCGA (0.74 mutations/Mb) samples (**Supplementary Fig. 2**). The mutation signature for the SNVs was similar to that found in GBMs and was predominated by typical age-related C>T transitions at CpG dinucleotides, except for the presence of mostly C(T/C)>T transitions in two cases (LGG6 and LGG270) who had been heavily treated with temozolomide, as previously reported[9] (**Supplementary Fig. 3**). After subtracting out regional background mutation rates[21], we initially identified 15 genes as being significantly mutated (false discovery rate (FDR) $q < 0.1$) (**Supplementary Table 4**). We obtained a more comprehensive list of significantly mutated genes by targeted sequencing of an additional 172 genes related to the above-mentioned genes or reported to be recurrently mutated in GBM[22–24], pediatric low-grade glioma[25] or pilocytic astrocytoma[26] in an independent set of 280 JPN samples (**Supplementary Tables 5** and **6**). We also investigated copy number variations (CNVs) using SNP array data sets for 291 JPN and 424 TCGA samples (**Fig. 1a**,**b** and **Supplementary Tables 7** and **8**),

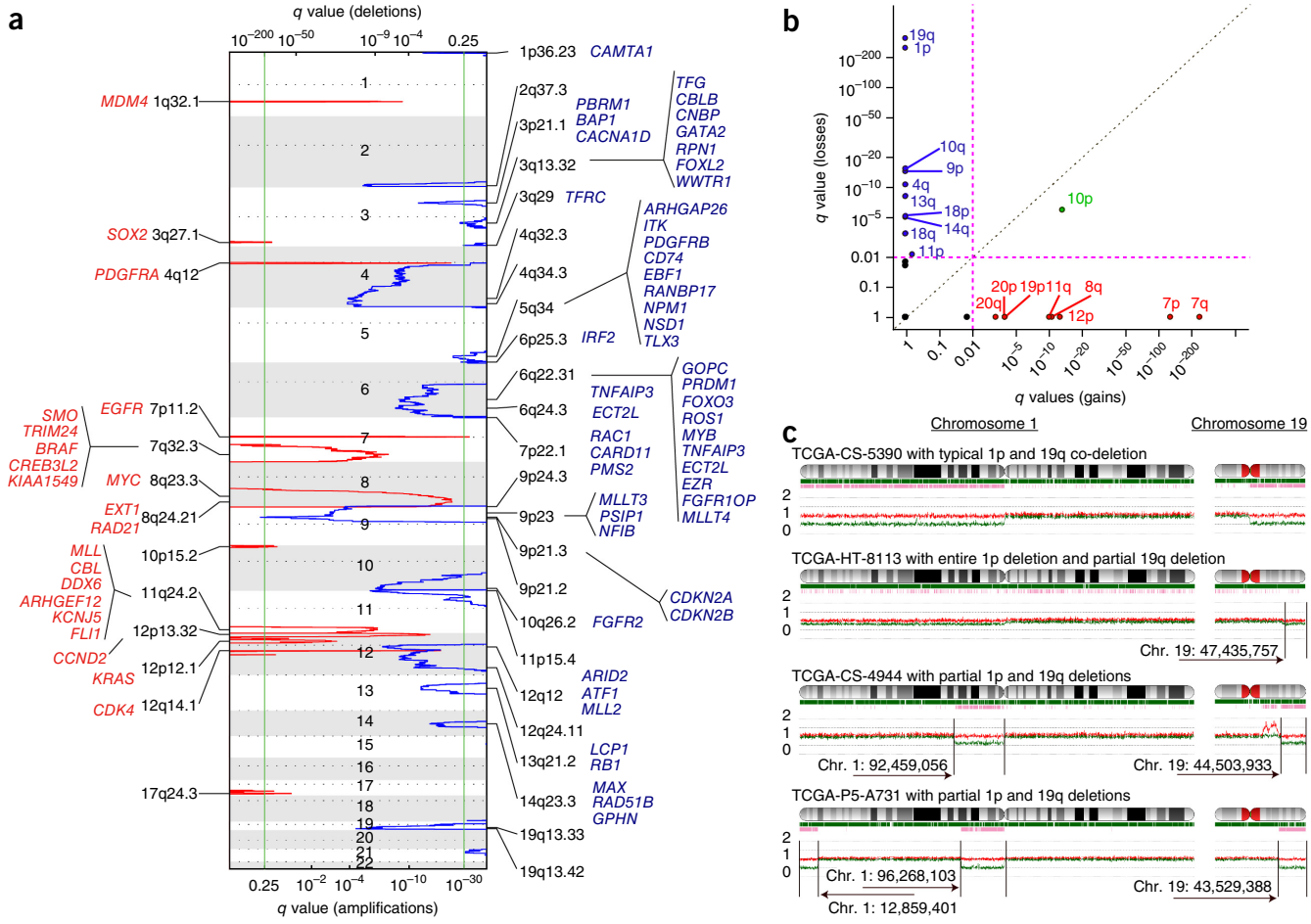


**Figure 1** Copy number alterations in grade II and III gliomas. (**a**) Significant copy number gains (red) and losses (blue) detected by analysis of the copy number data from the combined JPN and TCGA cohorts ($n = 717$) using GISTIC 2.0. Candidate gene targets within the corresponding loci are also indicated. (**b**) Significant arm-level copy number gains (red), losses (blue) and both (green). The magenta dashed lines represent significance (FDR $q = 0.01$). Frequently affected regions are indicated. (**c**) CNAG outputs for non-canonical 1p and 19q co-deletions, showing segmental deletions of 1p and 19q (ref. 54). The moving averages ($n = 10$) of allele-specific copy numbers are depicted in red (for larger alleles) and green (for smaller alleles). The positions of heterozygous SNP calls (green bars) and discordant SNP calls between tumor and normal samples (pink bars) are also shown. Vertical black lines indicate the position of breakpoints of deletions with exact genomic position.

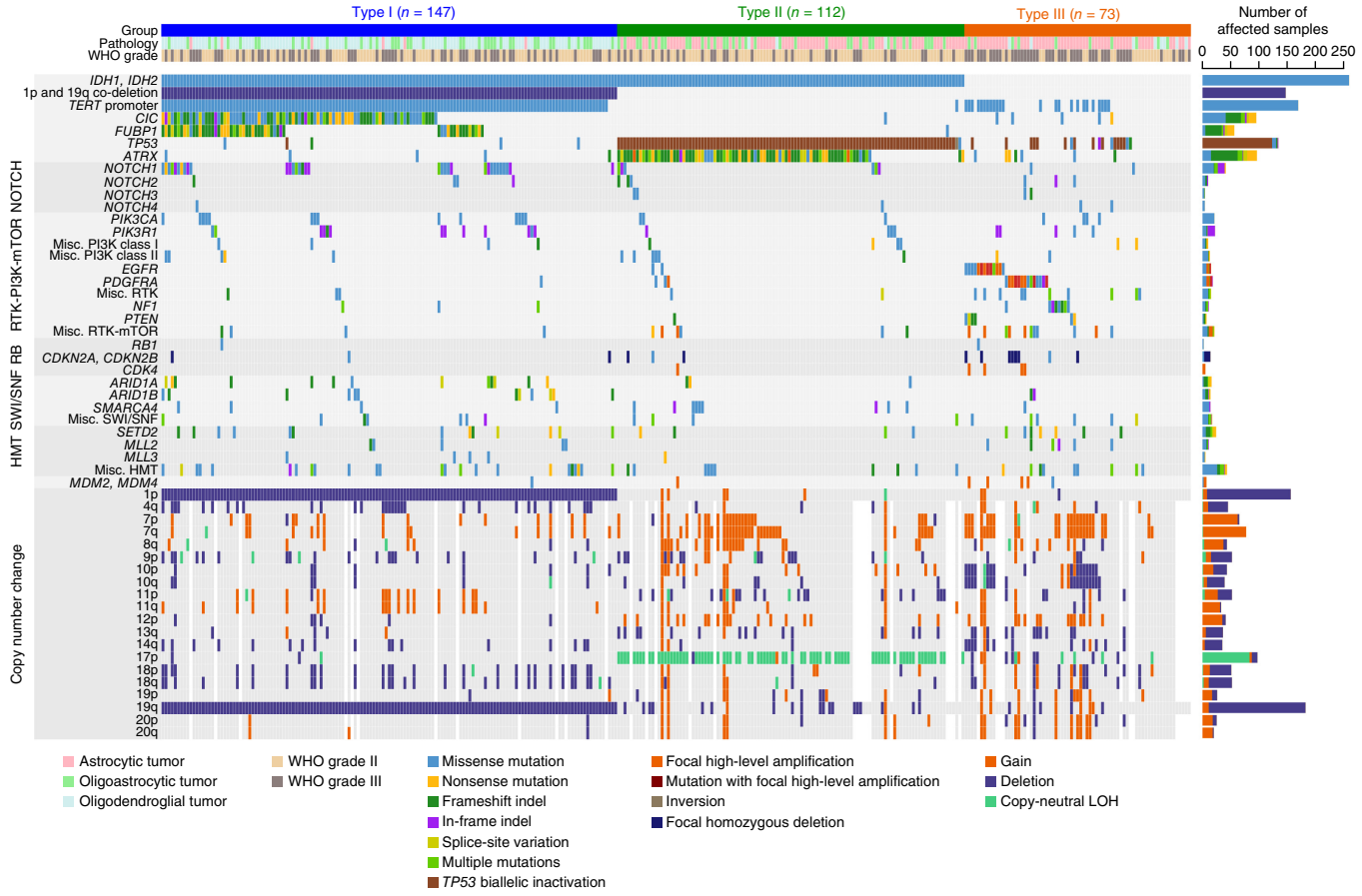


**Figure 2** Landscape of genetic lesions in grade II and III gliomas. The statistically significant genetic lesions in 332 grade II and III glioma cases from the JPN cohort are shown. Molecular classification, histology type and WHO grade (top rows) together with the numbers of affected cases and the types of mutations and CNVs are shown by color as indicated. Corresponding results for the TCGA ($n$ = 425) and combined ($n$ = 757) cohorts are provided in **Supplementary Figures 4** and **5**. PI3K, phosphatidylinositol 3-kinase; RTK, receptor tyrosine kinase; HMT, histone methyltransferase.



through which 37 focal regions and 19 chromosomal arms were shown to undergo recurrent copy number changes. In combination, a total of 58 genes were identified as being significantly affected by mutations and/or CNVs (**Fig. 1** and **Supplementary Tables 8–10**), on the basis of which we delineated the landscape of genetic lesions in the 2 grade II and III glioma cohorts (**Fig. 2** and **Supplementary Figs. 4** and **5**).

## Genetic features of grade II and III glioma subgroups

In total, 747 (98.7%) of the 757 samples in the entire cohort harbored at least one CNV or somatic mutation. Recapitulating previous reports[10,13–15,17,27,28], we confirmed frequent mutations in *IDH1*, the *TERT* promoter, *TP53*, *ATRX*, *CIC* and *FUBP1*, as well as 1p and 19q co-deletion, in the current study (**Fig. 2**). In both the JPN and TCGA cohorts, approximately three-fourths of the grade II and III glioma cases carried either an *IDH1* mutation or, in a much lower proportion of cases (<4%), an *IDH2* mutation (**Supplementary Table 11**). Mutually exclusive 1p and 19q co-deletion and *TP53* mutation are well-described accompanying lesions that characterize IDH-mutated gliomas and, regardless of WHO grade, have been implicated in oligodendroglial and astrocytic histology, respectively[27]. In fact, 1p and 19q co-deletion or *TP53* mutation was virtually an obligatory lesion in IDH-mutated tumors; in contrast to previous reports, in which as many as 4–24% of IDH-mutated cases had neither of these lesions[13,15,29], when we intensively scrutinized the sequencing and copy number data, all but 2 IDH-mutated tumors in the cohort had either 1p and 19q co-deletion or *TP53* inactivation (258/259 JPN and 341/342 TCGA samples) in a mutually exclusive manner. We found non-canonical 1p and 19q co-deletion events consisting of partial loss of a centromeric part of 1p and a telomeric part of 19q (ref. 30) in three TCGA subjects who lacked any detectable *TP53* lesions (**Fig. 1c**). Thus, in terms of the status of these relevant genetic lesions, grade II and III gliomas could be classified into exactly three, but no more, subtypes (types I–III) with only a few exceptional cases that had mutated IDH but lacked either 1p and 19q co-deletion or *TP53* lesions.

## Unique features of type I–III gliomas

Type I tumors, as defined by the presence of both IDH gene mutation and 1p and 19q co-deletion, had concomitant *TERT* promoter mutations in most cases (144/147 in the JPN cohort), with or without *CIC* (58% of type I cases) and/or *FUBP1* (31% of type I cases) mutations. All but one IDH-mutated tumor without 1p and 19q co-deletion (type II tumors) harbored mutated *TP53* with frequent coexisting *ATRX* mutation (77% of type II cases) but very rare *CIC* or *FUBP1* mutation (0.6% of type II cases) (77% of type II cases) and showed a significantly inferior overall survival rate in comparison to type I tumors (hazard ratio (HR) = 2.06, 95% confidence interval (CI) = 1.36–3.12) (**Fig. 3a**). Notably, although previously not recognized, *TP53* mutations in most type II cases (109/112 in the JPN cohort and 198/201 in the TCGA cohort) were accompanied by 17p

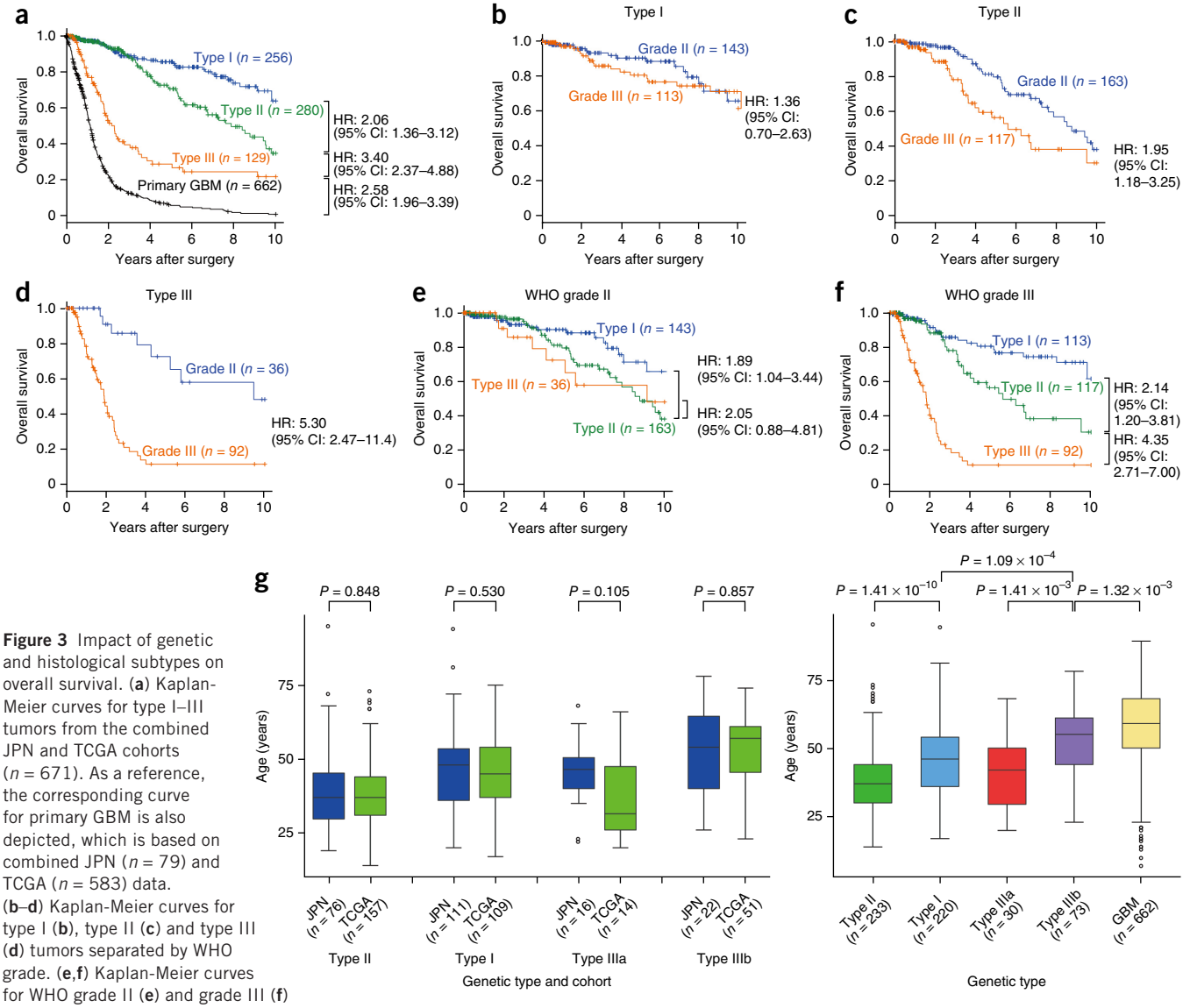


**Figure 3** Impact of genetic and histological subtypes on overall survival. (**a**) Kaplan-Meier curves for type I–III tumors from the combined JPN and TCGA cohorts ($n = 671$). As a reference, the corresponding curve for primary GBM is also depicted, which is based on combined JPN ($n = 79$) and TCGA ($n = 583$) data. (**b**–**d**) Kaplan-Meier curves for type I (**b**), type II (**c**) and type III (**d**) tumors separated by WHO grade. (**e**,**f**) Kaplan-Meier curves for WHO grade II (**e**) and grade III (**f**) tumors separated by genetic subtype. (**g**) The mean age at diagnosis for each genetic type and GBM is plotted with its 25% and 75% quartiles. Left, comparison of the JPN and TCGA cohorts. Right, comparison of the genetic subgroups and GBM. *P* values were calculated using the Wilcoxon rank-sum test. Each box plot shows the median with the 25–75% quartile range.

loss of heterozygosity (LOH), a second *TP53* mutation or complete loss of *TP53* expression, suggesting biallelic *TP53* inactivation. In contrast, all type I tumors with mutated *TP*53, if present, carried just a single dominant mutant allele with substantially lower variant allele frequency (VAF) than those for the alleles in type II tumors ($P = 4.5 \times 10^{-4}$, Wilcoxon rank-sum test).

The IDH–wild type, or type III, tumors comprised the remaining subgroup, accounting for 20.6% of grade II and III gliomas (156/757), of which approximately two-thirds were grade III tumors, especially anaplastic astrocytomas. In accordance with previous reports[10,31], type III gliomas represented the most aggressive tumors in the current cohort, showing an overall survival rate more similar to that of GBM, with a 29.1% rate of 5-year survival (**Fig. 3a**). Of particular interest was the finding that 113 of the 156 type III tumors were characterized by the presence of 'GBM-like' mutations and CNVs, such as amplification of *EGFR*, *PDGFRA*, *CDK4*, *MDM2* and *MDM4*, deletion or mutation of *PTEN*, *NF1*, *RB1*, *CDKN2A* and *CDKN2B*, del(10q), and amplification or mutation of class II phosphatidylinositol 3-kinase (PI3K) genes, which were much less frequent in type I and II tumors (**Fig. 2**).

WHO grade did not substantially affect overall survival within IDH-mutated (type I and II) tumors but did have an effect in type III tumors; grade III histology in particular, with evidence of anaplastic astrocytoma and oligoastrocytoma, was associated with very poor prognosis (HR = 6.41, 95% CI = 3.13–13.1) in comparison to grade II histology, which showed an overall survival rate comparable to those of type I and II tumors (**Fig. 3b–f** and **Supplementary Fig. 6**). In addition, grade III, type III gliomas comprised more astrocytic tumors (74/99 grade III tumors versus 21/43 grade II tumors; $P = 3.5 \times 10^{-3}$, Fisher's exact test), showed a higher mean age at diagnosis (52.3 versus 41.7 years of age in grade III and II tumors, respectively; $P = 1.4 \times 10^{-3}$) and had more GBM-like mutations ($P = 1.4 \times 10^{-3}$) in comparison to IDH–wild type, grade II tumors, suggesting that type III gliomas should be divided into 2 subtypes—grade II, type III (type IIIa) and grade III, type III (type IIIb) tumors. *BRAF*, *H3F3A* and *FGFR1* mutations, which are characteristic of pediatric grade I

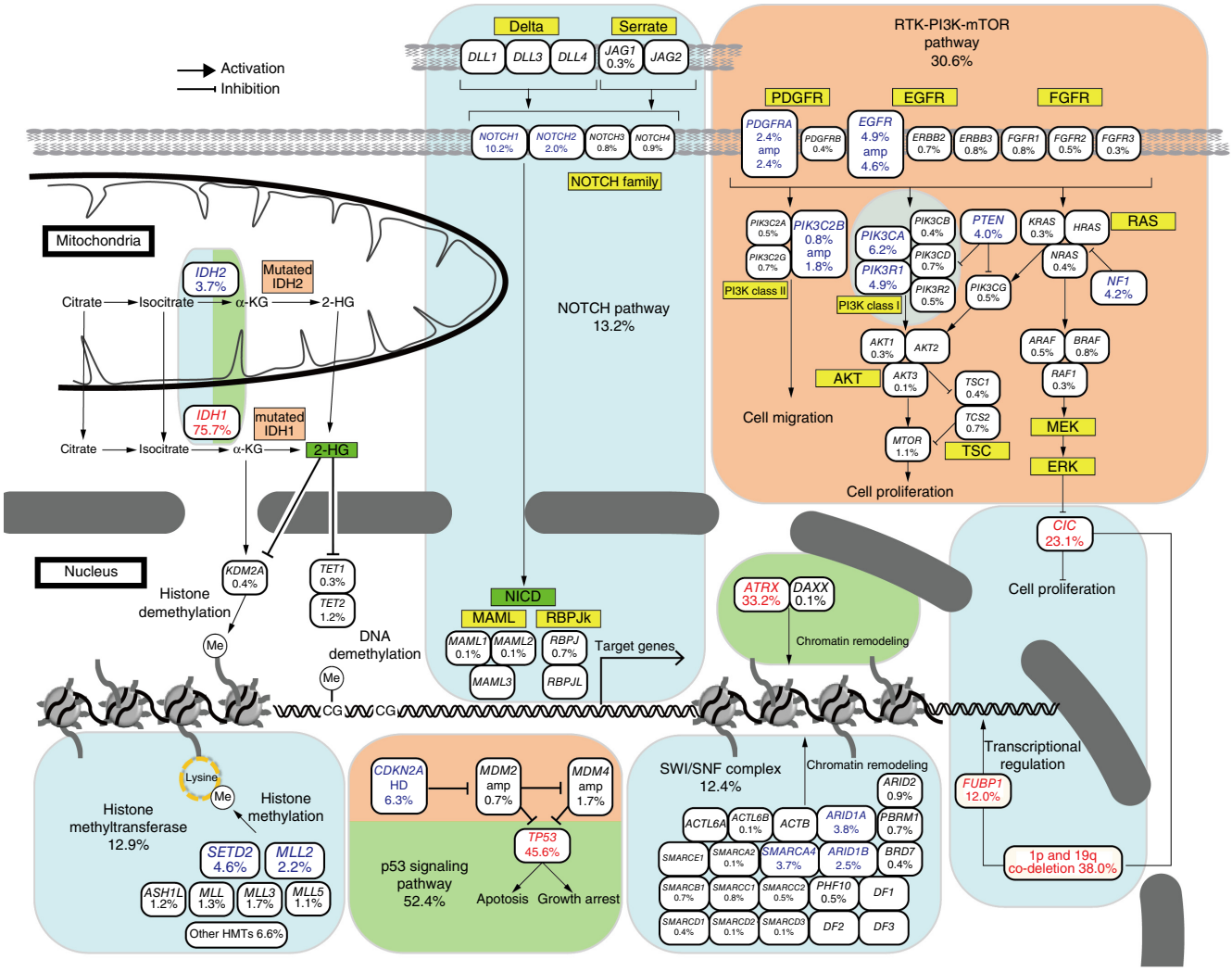


**Figure 4** Driver genes and functional pathways involved in grade II and III gliomas. Major functional pathways and their components affected by gene mutations and/or copy number changes in grade II and III gliomas are depicted. Alterations in type I (blue), type II (green) and type III (orange) tumors are specified. The frequency of each lesion is also indicated. Amp, focal high-frequency amplification; HD, homozygous deletion; α-KG, α-ketoglutarate; 2-HG, 2-hydroxyglutarate; NICD, Notch intracellular domain; Me, methyl group.

and II gliomas, were detected more in type IIIa tumors (4/43 grade II and 3/99 grade III cases), although the difference was not statistically significant. Type I–III gliomas were characterized by different mean ages at diagnosis for the patients; patients with type II tumors were significantly younger than those with type I tumors, and patients with type III gliomas—especially those with type IIIb tumors—had the highest mean age among the three groups but were still significantly younger than patients with GBM ($P = 1.32 \times 10^{-3}$, Wilcoxon rank-sum test) (**Fig. 3g**). We also evaluated the impact of other common mutations (mutation frequency >10%). In univariate analysis, *ATRX* mutation seemed to significantly affect overall survival, particularly in patients with astrocytoma, as previously reported[13,32]. However, in multivariate analysis, only genetic type, WHO grade and age were shown to independently affect overall survival, whereas *ATRX* mutation did not have a significant effect.

### Gene expression and DNA methylation in the TCGA cohort

We investigated the impact of major genetic alterations on DNA methylation and gene expression in grade II and III gliomas by downloading the corresponding data for the TCGA cohort. In DNA methylation profiling of grade II and III, as well as grade IV, gliomas, we identified three stable clusters (**Supplementary Fig. 7**). As previously reported, regardless of WHO grade and histology, IDH gene mutation strongly correlated with CpG island methylator phenotypes (CIMPs)[33], which were further affected by the status of 1p and 19q co-deletion and/or *TP53* mutation[34]. Thus, type I and II gliomas exactly conformed to the CIMP-A and CIMP-B subtypes, respectively, with a few exceptional samples: 2 IDH-mutated cases with non-canonical 1p and 19q co-deletion were marginally clustered with CIMP-B, together with one IDH–wild type GBM sample. Eight cases of IDH-mutated GBM were also clustered in CIMP-B, further suggesting a strong impact of IDH gene mutation on DNA methylation. Six of the eight cases were informative for gene mutation, of which six and four had *TP53* and *ATRX* mutations, suggesting that these IDH-mutated GBM cases evolved from type II astrocytic tumors. All type III glioma and other GBM samples were clustered together with the non-CIMP subtype without generating any discrete subclusters.

Similarly, we obtained four unique subgroups (S1–S4) based on gene expression clustering, although the clustering was much less stable and the separation of genotypes was less clear in comparison to

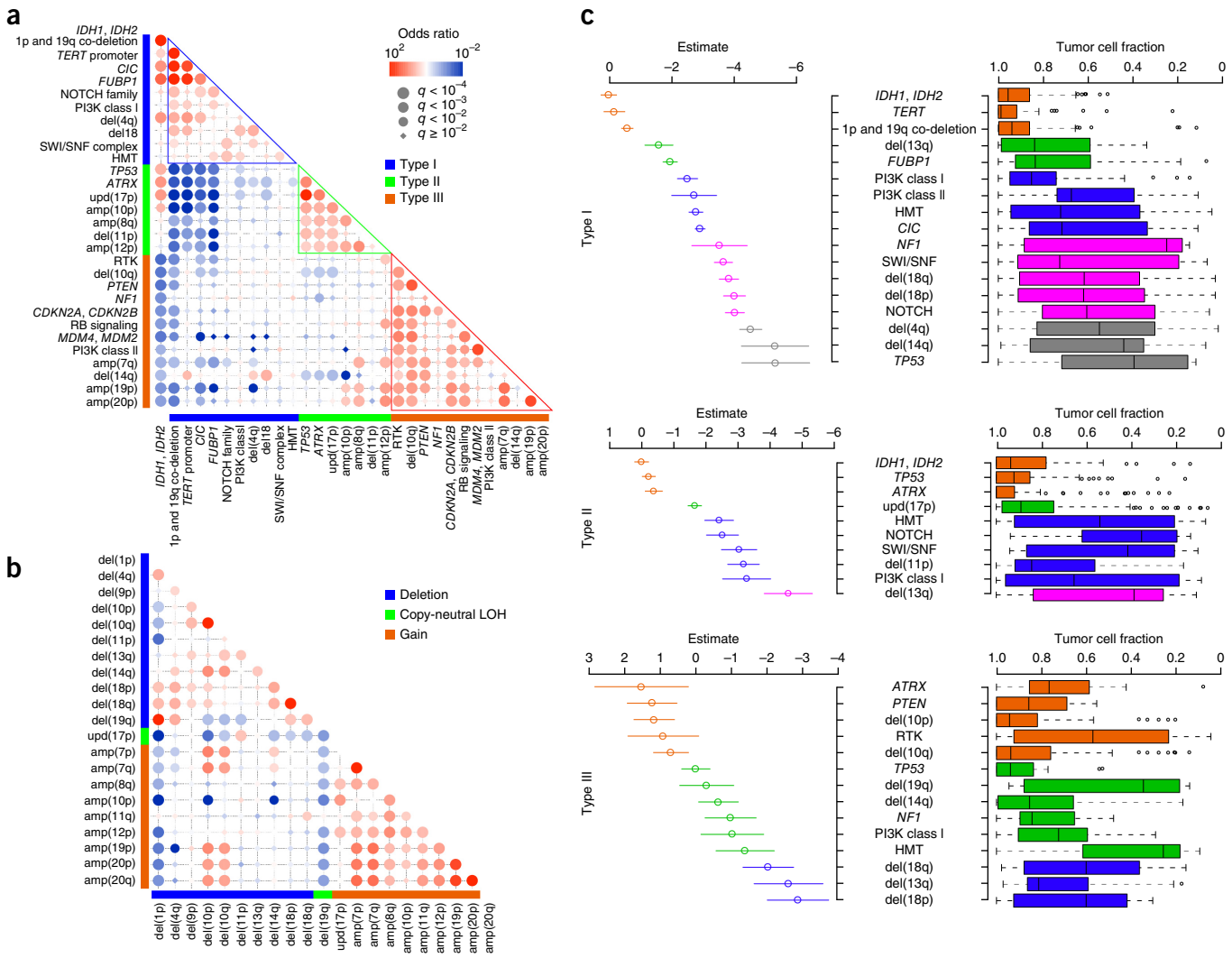


**Figure 5** Correlations and temporal hierarchy of gene alterations in grade II and III gliomas. (**a**,**b**) Statistically significant ($q < 0.01$) positive (red) and negative (blue) correlations among major driver mutations (**a**) and chromosomal gains and deletions (**b**) detected by exhaustive pairwise calculations of Fisher's exact test, where the size and color for each circle indicate the level of significance as expressed by the $q$ value and odds ratio of correlation, respectively. Multiple testing was adjusted for according to the Benjamini-Hochberg method. Genetic lesions relatively specific to type I, II or III tumors and largely positive correlations therein are indicated by colored bars. upd, uniparental disomy. (**c**) Temporal order of major lesions in type I, II and III tumors (top, middle and bottom left, respectively), with each expressed as the mean 'estimate' (±95% CI) calculated according to the Bradly-Terry model, where higher estimates indicate earlier events. The upper and lower quartiles ± 1.5 times the interquartile range (IQR) of the tumor cell fractions having the indicated lesions are also shown to the right.

that observed when considering DNA methylation (**Supplementary Fig. 8**). Nevertheless, we still observed strong correlation of genotype with clustering: IDH-mutated and IDH–wild type tumors were clustered separately in the S1–S3 and S4 subgroups, respectively, and S1 and S3 were mostly composed of type I and type II samples, respectively, whereas S2 was a highly heterogeneous admixture of different IDH-mutated samples. S4 contained most of the type III glioma and GBM samples, but these tended to form unique clusters within S4, strongly indicating that, in terms of gene expression, type III glioma and GBM cases are more similar than other subgroups but represent distinct sets of gliomas. Although Gene Set Enrichment Analysis (GSEA) did not identify specifically enriched gene sets in the S1, S3 and S4 subgroups, S2 was characterized by enrichment of genes whose promoters had high CpG content and showed dimethylation of histone H3 at lysine 4 (H3K4me2) and trimethylation of histone H3 at lysine 27 (H3K27me3) in neural progenitor cells ($q < 0.01$). We detected no other correlations of common genetic lesions with gene expression status.

## Other common driver genes in grade II and III gliomas

Additional driver alterations have been reported in several studies using relatively small cohorts of grade II and III gliomas, including in *NOTCH1* (refs. 14,28), *SETD2* (ref. 35) and *SMARCA4* (ref. 9), but have not been systematically investigated in a large cohort using next-generation sequencing. In the current study, the large number of enrolled samples allowed for the sensitive detection of common driver alterations in grade II and III gliomas and determination of their exact frequencies. The genome-wide landscape of driver lesions in grade II and III gliomas was largely similar for the JPN and TCGA cohorts, except for apparently lower mutation rates in *SETD2* and an even lower detection rate for *TERT* promoter mutations in the TCGA data, where very low coverage of the *TERT* promoter in whole-exome sequencing

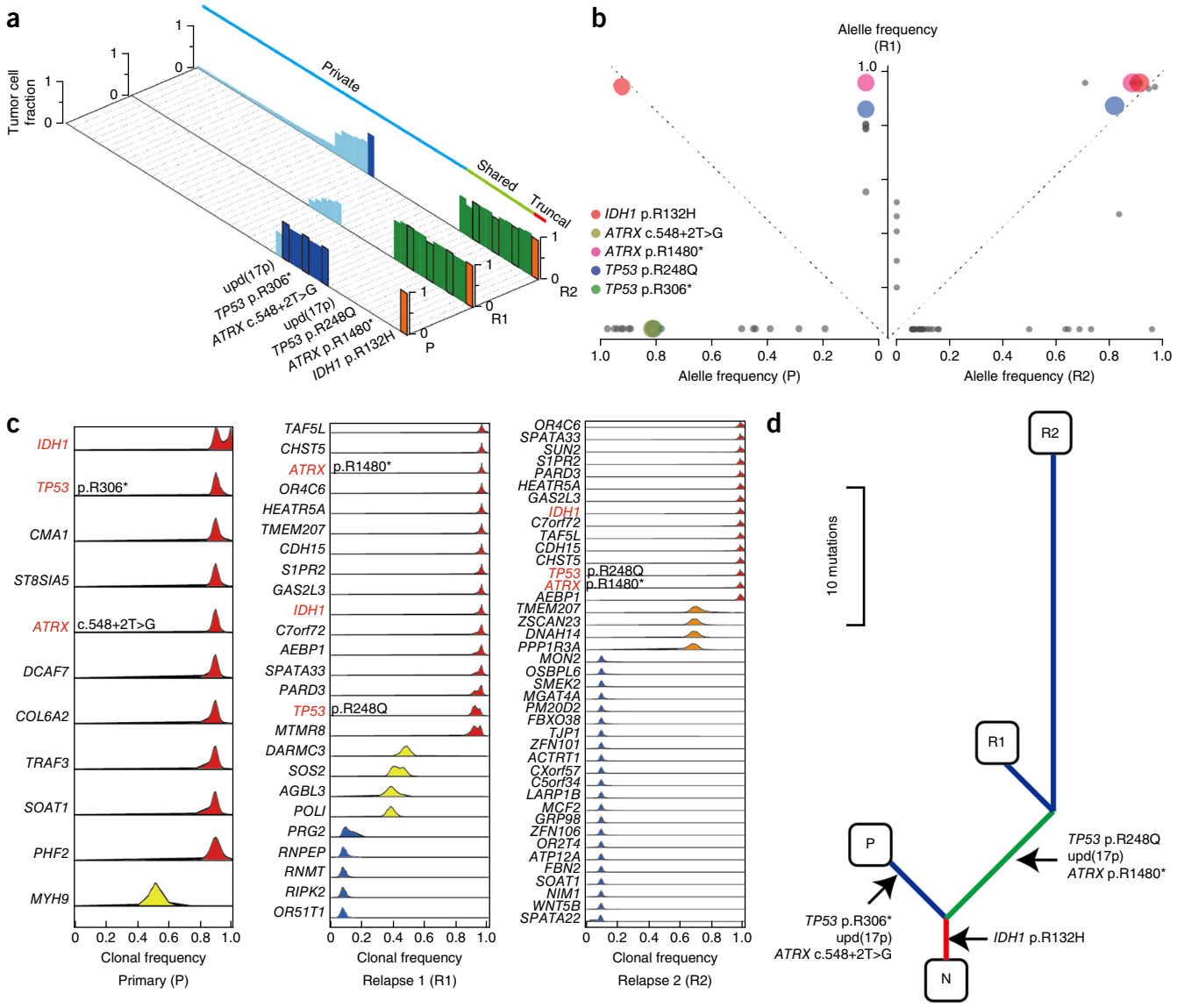


**Figure 6** Parallel evolution in serially collected samples. A representative case is shown having two sets of parallel mutations involving the *TP53* and *ATRX* genes, for which the primary tumor (P) and two relapse samples that occurred 1.6 (R1) and 36.2 (R2) months after diagnosis were consecutively collected and analyzed by whole-exome sequencing and subsequent deep sequencing. (**a**) Landscape of non-silent mutations and their burdens found in the primary and relapse tumors, in which mutations are either shared by all (orange) or only two (green) samples or are private to one of the three samples (blue, in which clonal and subclonal mutations are indicated in dark and light colors, respectively). (**b**) The VAFs of the mutations in the three samples are plotted on the left *x* axis (P), *y* axis (R1) and right *x* axis (R2) for comparison, focusing on mutation in *IDH1* and two parallel mutations. (**c**) On the basis of the results of deep sequencing, the estimated VAFs from the PyClone model are plotted for the sets of mutations found in three samples, showing multiple discrete subpopulations within each sample as indicated by color. (**d**) A phylogenetic tree demonstrates parallel evolution events harboring different *TP53* and *ATRX* mutations occurring between the isolation of the primary and relapse tumors. N, normal.

precluded sensitive detection of mutations (**Supplementary Figs. 4** and **9**, and **Supplementary Table 11**). Mutations in *NOTCH1*, a common driver gene in human cancers[36–39], were reported previously in small cohorts of patients with oligodendroglioma (4/16 and 2/7 cases[14,28]) and were observed in 41 of 332 (12.3%) JPN and 36 of 425 (8.5%) TCGA samples. Similar to other solid cancers but distinct from T cell malignancies, the gliomas had mutations that mapped to apparent hotspots within the EGF-like domains of NOTCH1 (**Supplementary Fig. 10e**). Including mutations in other related genes (*NOTCH1* homologs and their ligands and downstream molecules), NOTCH pathway genes were mutated in as many as 17% of samples in the JPN cohort and 10% of samples in the TCGA cohort (**Fig. 4**).

SETD2 belongs to the histone methyltransferases (HMTs), a family of proteins that have recently been reported to be mutated in human cancers, including gliomas[40,41]. *SETD2* and other HMT genes, such as *MLL1–MLL5* (also known as *KMT2A*, *KMT2D*, *KMT2C*, *KMT2B* and *KMT2E*, respectively) and *ASH1L*, were also common targets in grade II and III gliomas and were mutated in 13% (95/757) of the current cohort (**Fig. 4**). Other new mutational targets included multiple components of the SWI/SNF chromatin-remodeling complex (*ARID1A*, *ARID1B*, *SMARCA4* and other genes)[9] (13% or 95/757) and PI3K-mTOR pathway components (*PIK3CA*, *PIK3R1*, *PTEN* and *EGFR*) (31% or 232/757). We detected mutations in cell cycle regulators, including *CDKN2A*, *CDKN2B*, *RB1*, *CDK4* and *CCND2*, which

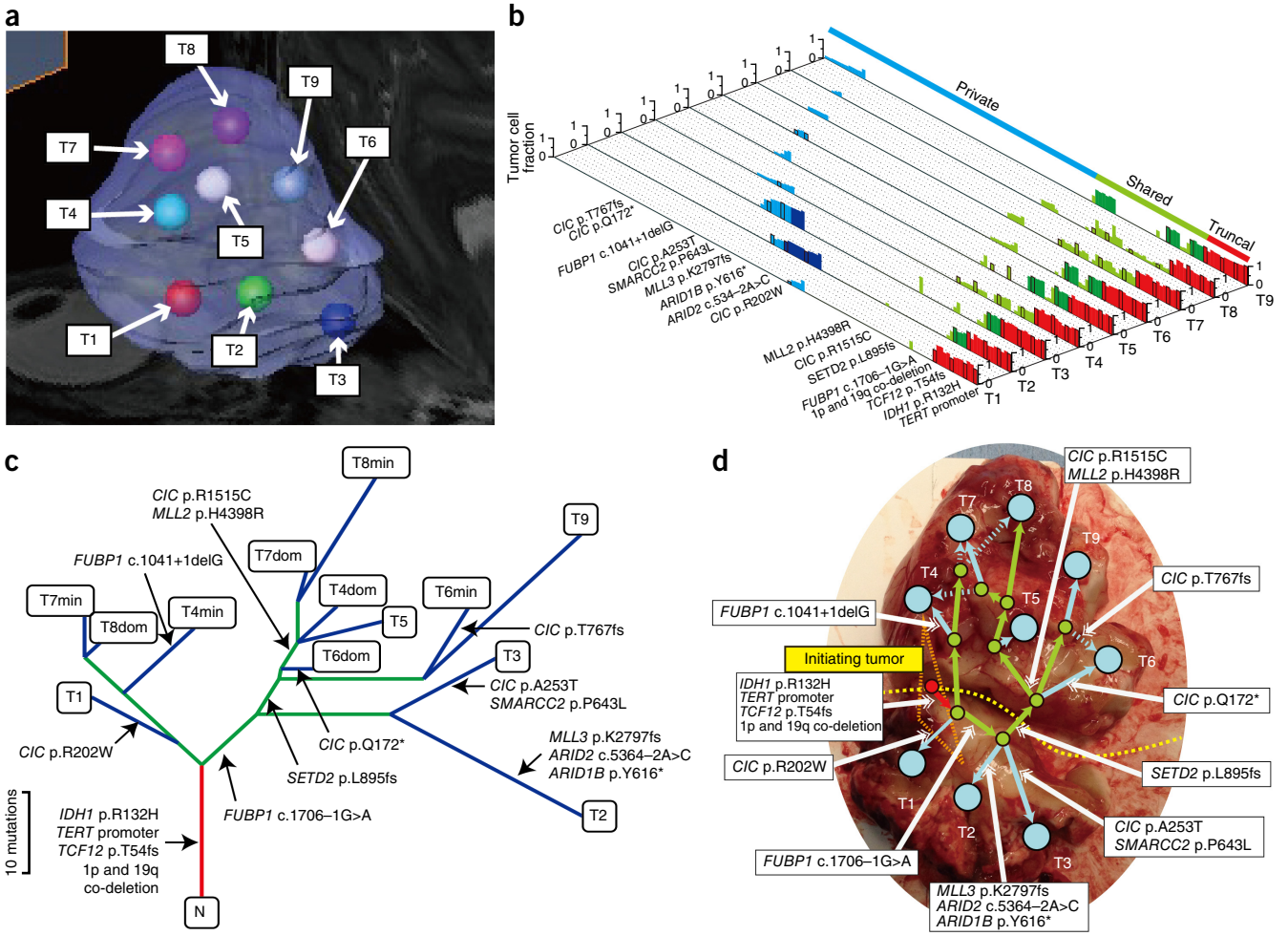


**Figure 7** Intratumoral heterogeneity and clonal evolution and expansion in grade II and III gliomas. (**a**) The positions of nine regional samplings (T1–T9) from case LGG174 are overlaid on a three-dimensional magnetic resonance image. (**b**) Landscape of genetic lesions in the nine regional samples, showing mutations shared by all samples (red), ones shared by partial subsets of samples (green) and non-shared, private mutations (blue). (**c**,**d**) The major driver and parallel mutations are mapped in a phylogenic tree (**c**), which is overlaid on the image of a real surgical specimen (**d**), where actual sampling sites (blue), imaginary evolutionary branch points (green) and a putative origin of tumor initiation (red) are indicated. The specimen was cut open down the middle (yellow line). Dom, dominant clone; min, minor clone.



were common targets of mutation and CNV in GBM, in 18.6% of grade II and III gliomas, especially in IDH–wild type (type III) samples, although the frequency was not as high as in GBM[22,24] (**Figs. 1a** and **4**). We identified two previously reported pathogenic gene fusions by interrogating RNA sequencing data from 417 TCGA grade II and III gliomas (Online Methods); *PTPRZ1-MET*[42] in 2 of 198 type II gliomas and *FGFR3-TACC3* (ref. 43) in 2 of 80 type III gliomas.

## Correlation of genetic alterations

The large number of samples also enabled the detection of significant correlations among different genetic lesions. In addition to the self-evident correlations among the core mutations that were highly specific to type I (IDH gene mutation combined with 1p and 19q co-deletion or mutation in the *TERT* promoter, *CIC* or *FUBP1*) and type II (IDH gene mutation combined with *TP53* or *ATRX* mutations) tumors, a number of statistically significant correlations were detected by exhaustive pairwise comparisons across major driver lesions (**Fig. 5a** and **Supplementary Fig. 11**). Notably, these genetic lesions were largely grouped into three major categories, corresponding to type I–III alterations, where mutations within the same category tended to show positive correlations, whereas those within different categories, especially core type I mutations relative to those in the type II and III categories, were globally mutually exclusive. An exception was significant positive correlation between del(14q) and *TERT* promoter mutations, del(4q) or del18 (**Fig. 5a**), reflecting an overall trend of positive correlations among recurrent gains and losses of several chromosome arms, including for 7q, 8q, 11q or 12p and 9p, 10q, 13q or 14q (FDR $q < 0.01$) (**Fig. 5b**). For example, mutations in class I PI3K components significantly coexisted with other type I mutations but were mutually exclusive with core type II mutations. Similarly, *NOTCH1* (or NOTCH family) mutations significantly coexisted with 1p and 19q co-deletion and mutations in the *TERT* promoter, *FUBP1*, the SWI/SNF complex and *MLL* (also known as *KMT2A*) or *SETD2*. Loss of 11p and gains of 8q, 10p and 12p correlated with *TP53* and *ATRX* mutations but were mutually exclusive with most of the core type I mutations. Frequently coexisting with del(10q), del(14q), amp(7q) and amp(20p), GBM-like mutations corresponded to type III lesions and tended to be mutually exclusive with most type I abnormalities. In combination, the presence of these strong correlations indicates that there is

functional interplay for particular combinations of genetic lesions during clonal evolution in grade II and III gliomas.

Moreover, there was also a significant difference in mean VAF among coexisting mutations that suggested the presence of a temporal order, although not always a stringent one, for mutations to occur (FDR $q < 0.01$) (**Fig. 5c**, right). We statistically evaluated the global trend in temporal order for mutations by comparing the VAFs of coexisting mutations on the basis of the Bradley-Terry model (**Fig. 5c**, left)[44]. Showing the largest VAFs in both type I and type II tumors, IDH gene mutations represented a founder event in these tumors, as was the case with *TERT* promoter mutations and 1p and 19q co-deletion alleles (in type I tumors) and *TP53* mutations (in type II tumors), which had indistinguishable VAFs from those of *IDH1* mutations. In contrast, mutations in *FUBP1*, *CIC*, *NOTCH1* and HMT genes, as well as in PI3K pathway genes, in type I tumors and *ATRX* mutations in type II tumors tended to have lower VAFs than *IDH1* mutations. We observed even lower VAFs for mutations in HMT genes, *CIC*, NOTCH pathway genes and the SWI/SNF complex in type I tumors and mutations in HMT genes, NOTCH pathway genes, the SWI/SNF complex and class I PI3K pathway genes in type II tumors, with these alterations representing later genetic events in the development of grade II and III gliomas. In type III tumors, mutations in *PTEN* and *ATRX*, as well as del(10q), were thought to be earlier events relative to mutations in HMT genes, class I PI3K components and del(14q), although the estimation of alteration order was more ambiguous than in type I and II tumors.

### Mutation studies by multiple regional and temporal sampling

We further investigated the temporal order of mutations during clonal evolution in grade II and III gliomas using serial sampling ($n = 10$) and multi-regional sampling (from 5–9 different sites within the same tumors; $n = 4$) (**Figs. 6** and **7**, **Supplementary Figs. 12** and **13**, and **Supplementary Table 12**), where whole-exome sequencing followed by targeted deep sequencing enabled the accurate estimation of the VAFs of the detected mutations, which could be used in constructing phylogenic trees (Online Methods). As in other cancer types[45–50], grade II and III gliomas showed substantial intratumoral heterogeneity: among four tumors for which multi-regional sampling was performed, only 9.2% of the observed mutations were shared by all samplings, whereas 58.1% of mutations were private to a single sampling (**Fig. 7b** and **Supplementary Fig. 13**). As expected from the above discussion, *IDH1* and *TERT* promoter mutations as well as 1p and 19q co-deletion in type I tumors were present in all regional and temporal samplings ($n = 9$), showing the highest VAFs within each sample, and were thus assigned as truncal events during tumor evolution, although we were unable to determine the relative order therein because there was no discordant sampling with respect to these mutations. In type II tumors, *IDH1*, *TP53* and, if present, *ATRX* mutations were truncal in most cases (4/5), except for case LGG5, in which 2 sets of independent *TP53* and *ATRX* mutations involved 2 major branches representing the primary tumor and 2 serially relapsed tumors, suggesting that, in this particular case, *TP53* and *ATRX* mutations were predated by *IDH1* mutation (**Fig. 6**). It was of interest that this tree represented a typical example of parallel mutations in cancer evolution, first described in clear cell renal cell carcinoma[46] and also reported recently in a single case with grade II glioma[9], in which multiple mutations involved the *SETD2* and *MTOR* genes and the *TP53* gene in parallel, suggesting that strong selective pressure fostered these mutations. We also found parallel mutations in the *CIC* (LGG1, LGG4 and LGG174), *FUBP1* (LGG174 and LGG202) and *NOTCH1* (LGG173) genes. Conspicuously, we detected a total of five different *CIC* mutations in all but one branch for LGG174, with or without accompanying independent *FUBP1* mutations and other mutations affecting the *SETD2*, *ARID1B*, *MLL2* and *SMARCC2* genes, indicating a critical role of *CIC* deregulation in the context of this particular tumor. Other type I alterations that appeared in peripheral branches included mutations in *MLL3* ($n = 4$), *ARID1A* ($n = 3$), *SETD1A* ($n = 2$), *SMARCA4* ($n = 1$) and *PIK3R1* ($n = 1$), as well as del(18p) ($n = 2$) and del(4q) ($n = 1$).

Finally, it was also intriguing that the phylogenetic branches in these tumors were closely associated with the spatial pattern of sampling in a manner that suggests contiguous tumor expansion (**Fig. 7d** and **Supplementary Fig. 13**). In LGG174, for instance, the original tumor was thought to arise from somewhere between sampling sites T1 and T4 (red circle) with *IDH1*, *TERT* promoter and *TCF12* mutations, together with 1p and 19q co-deletion, and propagated to T1, T4 and a common branch point for T2–T9 by acquiring mutations in *CIC* (p.Arg202Trp), *FUBP1* (c.1041+1delG) and *FUBP1* (c.1706–1G>A), respectively. The tumor then further expanded to T2 with mutations in *MLL3*, *ARID2* and *ARID1B*, to T3 with *CIC* (p.Ala235Thr) and *SMARCC2* mutations, to the common branch point for the dominant (*CIC* p.Gln172*) and minor (*CIC* p.Thr767fs) clones at T6, and to T5, T7 and T8 (*CIC* p.Arg1515Cys and *MLL2*), frequently showing confluence in the periphery between multiple components from surrounding branches at T4, T7 and T8 (**Fig. 7c**,**d**).

## DISCUSSION

Combining two large cohorts of grade II and III gliomas from Japan and the United States that were comprehensively analyzed by whole-exome sequencing and/or targeted deep sequencing as well as array comparative genomic hybridization (aCGH), to our knowledge, the current study provides the most complete description of genetic alterations in grade II and III gliomas ever reported. The large sample size enabled more comprehensive detection of driver alterations in grade II and III gliomas, as well as precise determination of their impact on pathophysiology and clinical outcomes. On the basis of the mutational status of *IDH1*, *IDH2* and other common lesions, grade II or III gliomas are divided into and exhausted by the genetically well-defined type I–III subtypes. Exhibiting characteristic sets of genetic lesions, mean age at diagnosis, histology, DNA methylation and gene expression patterns, and clinical behavior, these genetic subtypes may represent unique clinicopathological entities and, in combination with histology, may guide the better management of patients. Traditionally, grade III gliomas have been thought to be high-grade tumors associated with poor overall survival. However, grade III tumors in the type I or II subtype showed overall survival comparable to that of corresponding grade II tumors and therefore would be better managed as low-grade tumors; WHO grade does not seem to substantially affect overall survival, but the status of 1p and 19q co-deletion and *TP53* lesions significantly affects survival for IDH-mutated gliomas. Similarly, IDH–wild type (or type III) tumors frequently harbored GBM-like mutations and generally showed very poor prognosis, whereas grade II, type III tumors (type IIIa) were associated with substantially better overall survival in comparison to grade III, type III tumors (type IIIb).

The identity of type III glioma is another issue of particular interest that has been long discussed in the literature[10,51]. In terms of clinical outcome, pattern of mutations, DNA methylation, gene expression and histopathology, type III glioma is most similar to GBM and might represent misdiagnosed GBM; 3 JPN patients who had been initially diagnosed as having type III gliomas were rediagnosed as

having GBMs and excluded from the current study after central review. However, type III tumors showed significantly better overall survival, as recently reported[51], and lower mean age than GBMs and tended to be clustered in gene expression analysis separately from GBM samples. These results might argue that type III glioma represents a distinct entity from GBM, even though a minority could be bona fide GBM cases.

Statistical evaluation of the VAFs for coexisting mutations and mutation analyses in spatially and temporally separated specimens not only demonstrated very complex intratumoral heterogeneity but also underscores the presence of a hierarchy among these alterations, as recently demonstrated in myelodysplastic syndromes[52,53]. In particular, all mutations in *IDH1* and the *TERT* promoter as well as 1p and 19q co-deletion in type I tumors and most *TP53* and, if present, *ATRX* mutations in type II tumors were found in the common trunks of the phylogenetic trees in multiple and serial sampling analyses. Thus, these mutations were likely to represent events that are virtually necessary and sufficient to establish grade II and III gliomas, while subsequent tumor progression and recurrence would take place through the acquisition of additional alterations, which seemed to occur at random but were nevertheless characterized by conspicuous positive or negative correlations among different classes of mutations. In combination, these findings indicate that the clonal selection of mutations in grade II and III glioma pathogenesis is conditional, at least to some extent, on particular combinations of preexisting mutations, which in turn indicate the presence of underlying functional interactions between these mutations in promoting oncogenesis.

Multi-regional sampling analysis also identified a close correlation of regional heterogeneity with the history of clonal evolution, illustrating the way in which a tumor expands from its origin to surrounding regions while increasing intratumoral heterogeneity and spatially intermingling different evolutionary branches in the periphery. Despite the presence of parallel mutations involving common targets, the detection of prominent regional heterogeneity raises a potential concern that the sequencing of bulk tumor may not detect rare but important mutations and/or tumor cell subpopulations that are maintained at low levels. Finally, it is currently still unclear whether different tumor types are determined by different combinations of early founder events affecting common neuronal progenitors or reflect different cells of origin for glioma that favor specific combinations of mutations for clonal selection, and clarifying the origin of the different tumor types will be essential in understanding the pathogenesis of grade II and III gliomas.

**URLs.** The Cancer Genome Atlas (TCGA) Consortium, http://cancergenome.nih.gov/; Gene Set Enrichment Analysis (GSEA), http://www.broadinstitute.org/gsea/; Cancer Genomics Hub (CGHub), https://cghub.ucsc.edu/; TCGA data portal, https://tcga-data.nci.nih.gov/tcga/; Picard tools, http://broadinstitute.github.io/picard/; dbSNP, http://www.ncbi.nlm.nih.gov/SNP/; ESP6500, http://evs.gs.washington.edu/EVS/; 1000 Genomes Project, http://www.1000genomes.org/; Catalogue of Somatic Mutations in Cancer (COSMIC), http://cancer.sanger.ac.uk/cancergenome/projects/cosmic/; Integrative Genomics Viewer (IGV), http://www.broadinstitute.org/igv/; HapMap Project, http://hapmap.ncbi.nlm.nih.gov/; MapSplice 2, http://www.netlab.uky.edu/p/bioinfo/MapSplice2; PyClone, http://compbio.bccrc.ca/software/pyclone/.

## METHODS

Methods and any associated references are available in the online version of the paper.

**Accession codes.** Sequencing and SNP array data have been deposited in the European Genome-phenome Archive (EGA) under accession EGAS00001001044.

*Note: Any Supplementary Information and Source Data files are available in the online version of the paper.*


## ACKNOWLEDGMENTS

We thank Y. Mori, M. Nakamura and H. Higashi for their technical assistance. We gratefully acknowledge the TCGA Consortium and all its members for making their invaluable data publically available. We are grateful to all patients who generously agreed to participate in this study. This work was supported by a Grant-in-Aid for Scientific Research on Innovative Areas (S.O.; 22134006) and the Funding Program for World-Leading Innovative Research and Development on Science and Technology (S.O.) and by a Grant-in Aid for Scientific Research on Innovative Areas from the Ministry of Education, Culture, Sports, Science and Technology of Japan (A. Natsume; 23107010) and funding from the Japan Neurosurgical Society (A. Natsume; Basic Project Plan FY2012-2014).


## AUTHOR CONTRIBUTIONS

Experiments and data analysis were performed by H.S., K.A., Y. Sato, A. Natsume, F.O., T. Yamamoto, K.T., M.R., T. Yoshizato, K.K., K.Y., Y.N., A.S.-O., M.S. and Y.K. Specimens were provided by T.W., K.M., H.N., M.M., T.A. and Y.M. Bioinformatics analyses were performed by H.S., K.A., K.C., Y. Shiozawa, Y. Shiraishi, A. Niida, T.S., H.T. and S.M. Histological analysis was performed by R.W. and I.I. H.S., K.A. and A. Natsume contributed to the generation of the figures, and H.S., K.A., A. Natsume and S.O. prepared the manuscript.

## COMPETING FINANCIAL INTERESTS

The authors declare no competing financial interests.




1. Ostrom, Q.T. *et al.* CBTRUS statistical report: primary brain and central nervous system tumors diagnosed in the United States in 2006–2010. *Neuro-oncol.* **15** (suppl. 2), ii1–ii56 (2013).
2. Claus, E.B. & Black, P.M. Survival rates and patterns of care for patients diagnosed with supratentorial low-grade gliomas: data from the SEER program, 1973–2001. *Cancer* **106**, 1358–1363 (2006).
3. Louis, D.N. *et al.* The 2007 WHO classification of tumours of the central nervous system. *Acta Neuropathol.* **114**, 97–109 (2007).
4. Stupp, R. *et al.* Radiotherapy plus concomitant and adjuvant temozolomide for glioblastoma. *N. Engl. J. Med.* **352**, 987–996 (2005).
5. Stupp, R. *et al.* Effects of radiotherapy with concomitant and adjuvant temozolomide versus radiotherapy alone on survival in glioblastoma in a randomised phase III study: 5-year analysis of the EORTC-NCIC trial. *Lancet Oncol.* **10**, 459–466 (2009).
6. Bauman, G., Fisher, B., Watling, C., Cairncross, J.G. & Macdonald, D. Adult supratentorial low-grade glioma: long-term experience at a single institution. *Int. J. Radiat. Oncol. Biol. Phys.* **75**, 1401–1407 (2009).
7. Smith, J.S. *et al.* Role of extent of resection in the long-term outcome of low-grade hemispheric gliomas. *J. Clin. Oncol.* **26**, 1338–1345 (2008).
8. Omuro, A. & DeAngelis, L.M. Glioblastoma and other malignant gliomas: a clinical review. *J. Am. Med. Assoc.* **310**, 1842–1850 (2013).
9. Johnson, B.E. *et al.* Mutational analysis reveals the origin and therapy-driven evolution of recurrent glioma. *Science* **343**, 189–193 (2014).
10. Yan, H. *et al. IDH1* and *IDH2* mutations in gliomas. *N. Engl. J. Med.* **360**, 765–773 (2009).
11. Hartmann, C. *et al.* Type and frequency of *IDH1* and *IDH2* mutations are related to astrocytic and oligodendroglial differentiation and age: a study of 1,010 diffuse gliomas. *Acta Neuropathol.* **118**, 469–474 (2009).
12. Liu, X.Y. *et al.* Frequent *ATRX* mutations and loss of expression in adult diffuse astrocytic tumors carrying *IDH1*/*IDH2* and *TP53* mutations. *Acta Neuropathol.* **124**, 615–625 (2012).
13. Jiao, Y. *et al.* Frequent *ATRX*, *CIC*, *FUBP1* and *IDH1* mutations refine the classification of malignant gliomas. *Oncotarget* **3**, 709–722 (2012).
14. Bettegowda, C. *et al.* Mutations in *CIC* and *FUBP1* contribute to human oligodendroglioma. *Science* **333**, 1453–1455 (2011).
15. Killela, P.J. *et al. TERT* promoter mutations occur frequently in gliomas and a subset of tumors derived from cells with low rates of self-renewal. *Proc. Natl. Acad. Sci. USA* **110**, 6021–6026 (2013).
16. Kannan, K. *et al.* Whole-exome sequencing identifies *ATRX* mutation as a key molecular determinant in lower-grade glioma. *Oncotarget* **3**, 1194–1203 (2012).
17. Arita, H. *et al.* Upregulating mutations in the *TERT* promoter commonly occur in adult malignant gliomas and are strongly associated with total 1p19q loss. *Acta Neuropathol.* **126**, 267–276 (2013).

18. Shiraishi, Y. *et al.* An empirical Bayesian framework for somatic mutation detection from cancer genome sequencing data. *Nucleic Acids Res.* **41**, e89 (2013).
19. Sato, Y. *et al.* Integrated molecular analysis of clear-cell renal cell carcinoma. *Nat. Genet.* **45**, 860–867 (2013).
20. Yoshida, K. *et al.* Frequent pathway mutations of splicing machinery in myelodysplasia. *Nature* **478**, 64–69 (2011).
21. Lawrence, M.S. *et al.* Mutational heterogeneity in cancer and the search for new cancer-associated genes. *Nature* **499**, 214–218 (2013).
22. Cancer Genome Atlas Research Netowrk. Comprehensive genomic characterization defines human glioblastoma genes and core pathways. *Nature* **455**, 1061–1068 (2008).
23. Frattini, V. *et al.* The integrated landscape of driver genomic alterations in glioblastoma. *Nat. Genet.* **45**, 1141–1149 (2013).
24. Brennan, C.W. *et al.* The somatic genomic landscape of glioblastoma. *Cell* **155**, 462–477 (2013).
25. Zhang, J. *et al.* Whole-genome sequencing identifies genetic alterations in pediatric low-grade gliomas. *Nat. Genet.* **45**, 602–612 (2013).
26. Jones, D.T. *et al.* Recurrent somatic alterations of *FGFR1* and *NTRK2* in pilocytic astrocytoma. *Nat. Genet.* **45**, 927–932 (2013).
27. Okamoto, Y. *et al.* Population-based study on incidence, survival rates, and genetic alterations of low-grade diffuse astrocytomas and oligodendrogliomas. *Acta Neuropathol.* **108**, 49–56 (2004).
28. Yip, S. *et al.* Concurrent *CIC* mutations, *IDH* mutations, and 1p/19q loss distinguish oligodendrogliomas from other cancers. *J. Pathol.* **226**, 7–16 (2012).
29. Watanabe, T., Nobusawa, S., Kleihues, P. & Ohgaki, H. *IDH1* mutations are early events in the development of astrocytomas and oligodendrogliomas. *Am. J. Pathol.* **174**, 1149–1153 (2009).
30. Vogazianou, A.P. *et al.* Distinct patterns of 1p and 19q alterations identify subtypes of human gliomas that have different prognoses. *Neuro-oncol.* **12**, 664–678 (2010).
31. van den Bent, M.J. *et al. IDH1* and *IDH2* mutations are prognostic but not predictive for outcome in anaplastic oligodendroglial tumors: a report of the European Organization for Research and Treatment of Cancer Brain Tumor Group. *Clin. Cancer Res.* **16**, 1597–1604 (2010).
32. Wiestler, B. *et al.* ATRX loss refines the classification of anaplastic gliomas and identifies a subgroup of *IDH* mutant astrocytic tumors with better prognosis. *Acta Neuropathol.* **126**, 443–451 (2013).
33. Noushmehr, H. *et al.* Identification of a CpG island methylator phenotype that defines a distinct subgroup of glioma. *Cancer Cell* **17**, 510–522 (2010).
34. Wiestler, B. *et al.* Integrated DNA methylation and copy-number profiling identify three clinically and biologically relevant groups of anaplastic glioma. *Acta Neuropathol.* **128**, 561–571 (2014).
35. Fontebasso, A.M. *et al.* Mutations in *SETD2* and genes affecting histone H3K36 methylation target hemispheric high-grade gliomas. *Acta Neuropathol.* **125**, 659–669 (2013).
36. Mantha, S. *et al.* Activating *Notch1* mutations are an early event in T-cell malignancy of *Ikaros* point mutant *Plastic/+* mice. *Leuk. Res.* **31**, 321–327 (2007).
37. Cancer Genome Atlas Research Network. Comprehensive genomic characterization of squamous cell lung cancers. *Nature* **489**, 519–525 (2012).
38. Agrawal, N. *et al.* Exome sequencing of head and neck squamous cell carcinoma reveals inactivating mutations in *NOTCH1*. *Science* **333**, 1154–1157 (2011).
39. Weng, A.P. *et al.* Activating mutations of *NOTCH1* in human T cell acute lymphoblastic leukemia. *Science* **306**, 269–271 (2004).
40. Dalgliesh, G.L. *et al.* Systematic sequencing of renal carcinoma reveals inactivation of histone modifying genes. *Nature* **463**, 360–363 (2010).
41. Zhu, X. *et al.* Identification of functional cooperative mutations of *SETD2* in human acute leukemia. *Nat. Genet.* **46**, 287–293 (2014).
42. Bao, Z.S. *et al.* RNA-seq of 272 gliomas revealed a novel, recurrent *PTPRZ1-MET* fusion transcript in secondary glioblastomas. *Genome Res.* **24**, 1765–1773 (2014).
43. Di Stefano, A.L. *et al.* Detection, characterization and inhibition of *FGFR-TACC* fusions in *IDH* wild type glioma. *Clin. Cancer Res.* doi:10.1158/1078-0432.CCR-14-2199 (21 January 2015).
44. Lancaster, J.F. & Quade, D. Random effects in paired-comparison experiments using the Bradley-Terry model. *Biometrics* **39**, 245–249 (1983).
45. Ding, L. *et al.* Clonal evolution in relapsed acute myeloid leukaemia revealed by whole-genome sequencing. *Nature* **481**, 506–510 (2012).
46. Gerlinger, M. *et al.* Intratumor heterogeneity and branched evolution revealed by multiregion sequencing. *N. Engl. J. Med.* **366**, 883–892 (2012).
47. Yachida, S. & Iacobuzio-Donahue, C.A. Evolution and dynamics of pancreatic cancer progression. *Oncogene* **32**, 5253–5260 (2013).
48. Wang, Y. *et al.* Clonal evolution in breast cancer revealed by single nucleus genome sequencing. *Nature* **512**, 155–160 (2014).
49. Zhang, J. *et al.* Intratumor heterogeneity in localized lung adenocarcinomas delineated by multiregion sequencing. *Science* **346**, 256–259 (2014).
50. de Bruin, E.C. *et al.* Spatial and temporal diversity in genomic instability processes defines lung cancer evolution. *Science* **346**, 251–256 (2014).
51. Hartmann, C. *et al.* Patients with *IDH1* wild type anaplastic astrocytomas exhibit worse prognosis than *IDH1*-mutated glioblastomas, and *IDH1* mutation status accounts for the unfavorable prognostic effect of higher age: implications for classification of gliomas. *Acta Neuropathol.* **120**, 707–718 (2010).
52. Haferlach, T. *et al.* Landscape of genetic lesions in 944 patients with myelodysplastic syndromes. *Leukemia* **28**, 241–247 (2014).
53. Papaemmanuil, E. *et al.* Clinical and biological implications of driver mutations in myelodysplastic syndromes. *Blood* **122**, 3616–3627 quiz 3699 (2013).

## ONLINE METHODS

**Subjects and materials.** The study included two large cohorts of grade II and III gliomas from Japan (JPN) and the United Sates (TCGA). The JPN cohort consisted of 335 cases, which had been diagnosed by local pathologists as grade II or III gliomas at Nagoya University, Kumamoto University, Kyushu University, Oita University or Tokyo Women's Medical University. All tumor samples were collected at the time of surgery after informed consent was obtained. Genomic DNA was isolated from both tumor and matched normal specimens, where peripheral blood was used as a germline control. For 304 samples, histological specimens were available for central review by 2 board-certified pathologists according to WHO classification to confirm that the tumor specimens were histologically consistent with diffuse astrocytoma, oligoastrocytoma, oligodendroglioma, anaplastic astrocytoma, anaplastic oligoastrocytoma or anaplastic oligodendroglioma, through which evaluation 3 samples were rediagnosed as GBM and thus excluded from the analysis. This study was approved by the ethics committees at all the participating institutes. The clinical courses of the cases for which serial samples were collected are shown in **Supplementary Table 12**. Information on the TCGA cohort is available from the TCGA data portal.

**Whole-exome sequencing and mutation calling.** Whole-exome sequencing was performed using targeted capture of all exon sequences with SureSelect Human All Exon v4 or v5 (Agilent Technologies) followed by massively parallel sequencing of enriched exon fragments on the HiSeq 2000 or 2500 platform (Illumina) using 100-bp paired-end mode, as previously described[20]. Whole-exome sequencing data were uniformly processed to obtain a list of somatic mutations from the fastq files. To this end, we needed to convert BAM files to fastq files because only BAM files were available for the TCGA data. Thus, the BAM files for 425 paired tumor-normal samples were downloaded from the Cancer Genomics Hub (CGHub) under accession 25614-3, which were first converted back to fastq files, where the 'read1' and 'read2' entries in the fastq files were reconstructed on the basis of paired-read information. For reverse-strand reads, we generated complementary bases and assigned BaseQuality scores accordingly. In this process, reads that had a flag of "not primary alignment," "read fails platform/vendor quality checks" or "supplementary alignment" were discarded using SAMtools 0.1.18.

Sequencing reads were first aligned to NCBI Human Reference Genome Build 37 (hg19) using the Burrows-Wheeler Aligner, version 0.5.8, with default parameter settings. PCR duplicates were eliminated using Picard tools version 1.39. Mutation calling was performed using the Empirical Bayesian Mutation Calling (EBCall) algorithm with the following parameters[18]: (i) Mapping Quality score ≥30; (ii) BaseQuality score ≥15; (iii) tumor and normal depths both ≥8; (iv) number of variant reads in tumors ≥2; (v) VAFs in tumor samples ≥0.05; and (vi) VAFs in normal samples ≤0.05. We used stringent criteria for mutation calling, requiring a $P$ value (by EBCall[18]) $<10^{-5.5}$ and a Fisher's $P$ value $<10^{-2.5}$, as determined by counting the number of reads with the reference base and the candidate SNV in both the tumor and normal samples as validated mutations.

**Validation of candidate variants.** Candidate variants were validated by targeted capture of the detected variants or PCR amplification of the corresponding reads, followed by high-throughput sequencing. Targeted gene capture was accomplished using the SeqCap EZ library (Roche NimbleGen) for custom bait. Sequencing errors were evaluated by calculating the standard deviation score (SD score) for each variant. The SD score for the $i$th variant ($S_i$) was defined as:

$$S_i = \frac{(F_i - M_i)}{D_i}$$

where $F_i$, $M_i$ and $D_i$ denote the VAF in the tumor sample and the mean and standard deviation of the number of variant reads at the mutated position in normal samples ($n = 15$), respectively. Candidate variants were considered to be validated when the VAF in the tumor sample was 5 times the VAF in the paired normal sample, $S_i$ was ≥8 or the number of variant reads in the tumor sample was ≥4.

PCR-based deep sequencing was performed as previously described[20]. Candidate mutations were thought to be real if all the following criteria were satisfied: (i) the VAF in the tumor was at least 5 times the VAF in the normal sample; (ii) the VAF in the paired normal sample was <0.005; and (iii) the sequencing depth was ≥2,500. In total, 786 candidate mutations found in 33 samples were selected for validation, of which 768 (97.7%) were validated. Significantly mutated genes ($q < 0.1$) were identified on the basis of the combined set of mutations observed in the combined JPN and TCGA data, using MutSigCV[21] with its default setting (**Supplementary Table 4**).

**Targeted resequencing of candidate drivers.** We selected 185 genes for the custom bait library (**Supplementary Table 5**), which included (i) significantly mutated genes detected by MutSigCV; (ii) genes that were reported to interact with or be in the same family as significantly mutated genes; (iii) genes that were recurrently mutated in GBM[22–24], pediatric low-grade glioma[25] and pilocytic astrocytoma[26]; and (iv) genes that were reported to be involved in chromatin remodeling, cell migration or the regulation of apoptosis. Fragmented genomic DNA was ligated with Illumina adaptors, indexed with the Next Ultra DNA Library Prep Kit for Illumina (New England BioLabs) and enriched using the SeqCap EZ library designed to capture all coding exons of the 185 target genes and the promoter region of *TERT*, according to the manufacturer's protocol. Enriched targets were sequenced according to the methods described for whole-exome sequencing.

**Mutation calling for targeted sequencing data.** Sequencing reads were aligned as described for whole-exome sequencing, where reads that had either a Mapping Quality score of <25, a BaseQuality score of <30 or ≥5 mismatched bases were excluded from the analysis.

To exclude sequencing errors, all nucleotide bases were enumerated at each nucleotide position within the target sequences (575,140 bp ($S$)), and the error rate per base ($E$) for each sample was calculated as the fraction of erroneous bases out of the total number of bases, where all bases other than the most frequent base were considered to be sequencing errors. Assuming a Poisson distribution, variants were considered to be sequencing errors if the number of supporting reads was less than the minimum $k$ value ($k_{\min}$) that held the condition $SE^k e^{-E}/k! < 0.01$ or the VAF was less than or equal to $k_{\min}$/mean depth. All variants that were supported by single-direction reads were excluded.

The following were also excluded: (i) synonymous mutations and variants without complete ORF information; (ii) missense SNVs that were registered in public and private databases, including dbSNP131, ESP6500, the 1000 Genomes Project as of April 2012 and our in-house database (because some pathogenic SNVs are registered in these databases, we recovered SNVs that had more than ten entries at the identical genomic position and a substituted base in the Catalogue of Somatic Mutations in Cancer (COSMIC) v67); (iii) all variants found in normal samples ($n = 240$) showing allele frequencies >0.0025; and (iv) all variants in paired samples showing VAFs ≥0.1 in the normal sample.

In non-paired samples, the following variants were considered to be somatic mutations: variants with $0.4 \leq \text{VAF} \leq 0.6$ that (i) were either nonsense, indel or splice-site variations, (ii) affected the same position in any other samples, (iii) were found at the same position in TCGA GBM cases, (iv) were registered for more than ten counts at the same position in COSMIC v67, (v) were located within the hotspot domains in *TP53*, *ATRX*, *CIC*, *NOTCH1* or *SMARCA4* (**Supplementary Table 13**) or (vi) were computationally predicted by SIFT (score < 0.05), PolyPhen-2 (damaging) and MutationAssessor (high or medium) to have negative functional consequences. All variants with $0.3 \leq \text{VAF} < 0.4$ or $0.6 < \text{VAF} \leq 0.7$ that were not predicted as 'benign', and all variants with VAF < 0.3 or VAF > 0.7 were considered as somatic mutations.

Finally, mapping errors were removed by visual inspection on the Integrative Genomics Viewer (IGV) browser. When the above criteria were applied to data from paired samples ($n = 201$) for validation, 949 of 989 (95.1%) true positive somatic variants were detected with a sensitivity of 96.0% (949/989).

**Detection of *TERT* promoter mutations by Sanger sequencing.** Because of the frequent low coverage of the *TERT* promoter region in exome sequencing, we performed Sanger sequencing or PCR-based deep sequencing to detect *TERT* promoter mutations in those samples that had <25× coverage at the mutational hotspots (chr. 5: 1,295,228 and 1,295,250). Primer sequences are shown in **Supplementary Table 14**. Sanger sequencing was performed using the 3130xl Genetic Analyzer (Applied Biosystems) according to the manufacturer's

protocol. Results are summarized in **Supplementary Table 15**. In TCGA samples, missing data on the status of *TERT* promoter mutations were imputed using the mi R package (0.09-18.03) for analysis of the correlation of genetic alterations in grade II and III gliomas. In total, 23 variables were selected for imputation, including genetic type (types I–III), mutated genes detected in more than 30 samples and CNVs observed in more than 70 samples in the combined JPN and TCGA samples.

**Targeted deep sequencing of PCR-amplified fragments for mutations and SNPs.** Mutations in the *IDH1*, *IDH2*, *TP53* and *ATRX* genes were investigated by deep sequencing of PCR-amplified DNA for 315 Japanese samples. To enable the random reading of targeted sequences, we first amplified the target sequences using primers tagged with NotI cleavage sites, and the products were then ligated and fragmented for deep sequencing as previously described[20]. To estimate the cancer cell fraction harboring 1p and 19q co-deletion or 17p LOH, we also carried out deep sequencing of multiple SNP sites (at least five highly heterozygous SNPs) on chromosomes 1p, 19q and 17p and calculated the cancer cell fractions on the basis of the observed VAFs. SNPs were selected that were present in a coding exon and showed a minor allele frequency of >0.3 in the Japanese population in HapMap Data Release 28 (Phases II and III), removing SNPs in repeat regions. Primer sequences and the results are shown in **Supplementary Tables 15** and **16**.

**Detection of significantly mutated genes on the basis of validation sequencing.** The significance of the mutations in each gene was evaluated by calculating type I error under the null hypothesis that all the non-silent mutations were passenger changes, assuming a Poisson distribution with a uniform background mutation rate ($\lambda$). For conservative evaluation, we employed $\lambda = 1$ mutation/Mb, although the observed mutation rate in whole-exome sequencing was 0.74 mutations/Mb. After calculating the type I errors for 185 genes, significantly mutated genes ($q < 0.01$) were estimated according to standard methods by Benjamini-Hochberg.

**SNP array analysis.** We assessed the genome-wide copy number alterations for 291 tumors using GeneChip Human Mapping 250K NspI or CytoScan HD arrays (Affymetrix) according to the manufacturer's instructions. We also downloaded SNP array data for the TCGA samples to analyze genomic copy number, and the JPN and TCGA data were uniformly analyzed for CNVs using CNAG[54,55]. Significant focal CNVs ($q < 0.25$) were detected using GISTIC 2.0. For GISTIC analysis, the different probe sets for the different array platforms (250K NspI, CytoScan HD and SNP Array 6.0) were adjusted by uniformly using the 250K NspI SNPs as surrogates for SNPs that were marginally located within the abnormal copy number segments on the CytoScan HD and SNP Array 6.0. Within each focal CNV, a gene was considered to be a significant target when it was registered in the Cancer Gene Census and had more than 30 entries in COSMIC v70. Results are shown in **Supplementary Table 10**. We also tested the significance of copy number alterations on chromosomal arms on the basis of Poisson binomial statistics as previously described[56]. Arm-level aberrations with $q < 0.01$ were considered to be significant.

**Gene fusion identification.** We downloaded 417 fastq files for RNA sequencing from CGHub and used MapSplice 2 to detect fusion genes with the default setting. We considered a junction to be true if at least four reads were aligned to the junction and both junction sites were not located in repeat lesions.

**Clustering for DNA methylation.** DNA methylation data for 425 grade II and III glioma and 144 GBM samples were downloaded from the TCGA data portal, and the combined data sets were analyzed.

Beta-mixture quantile normalization was performed to correct for probe design bias in the Illumina Infinium HumanMethylation450 BeadChip data. Of the >480,000 probes on the methylation chip, we selected probes that were annotated with "Promoter_Associated" or "Promoter_Associated_Cell_type_specific" and were designed in "Island," "N_Shore" or "S_Shore" regions, removing those designed on the X and Y chromosomes and those with >10% missing values.

After filtering these non-relevant probes, 80,057 probes were retained for further analysis. Missing values were estimated with the Bioconductor package pcaMethods. Consensus clustering was performed using hierarchical clustering based on the Ward and Pearson correlation algorithms with 1,000 iterations on the top 1% (4,856) of probes showing high variation by median absolute deviation (MAD) across the data set using the Bioconductor package ConsensusClusterPlus. The number of clusters was determined by the relative change in area under the cumulative distribution function curve by consensus clustering.

**Clustering for gene expression.** RNA sequencing data for 422 grade II and III glioma and 160 GBM samples were available from the TCGA data portal, in which sequencing reads were normalized to estimates of gene expression for 20,531 genes. After excluding genes for which normalized gene estimates were low (≤25th percentile relative to the median), a total of 1,500 genes were selected with a MAD of normalized gene estimates for expression profiling. Combined grade II–IV glioma samples were subjected to consensus clustering, which was performed using the same methods as with DNA methylation analysis. To characterize expression subclasses, we used the GSEA tool[57].

**Correlation of genetic alterations.** Correlations between mutations and CNVs were investigated by Fisher's exact test, in which mutated genes were grouped into 10 categories by their functionalities (**Supplementary Table 5**)[22,58,59]. We performed exhaustive pairwise testing across 6 single genes (*TP53*, *ATRX*, *CIC*, *FUBP1*, *PTEN* and *NF1*), the *TERT* promoter, the 10 categories of genes and 13 copy number changes in chromosomal arms. Multiple testing was corrected for by the method proposed by Benjamini-Hochberg, in which $q < 0.01$ was considered to be significant. We also investigated correlations exclusively between copy number changes on chromosomal arms.

**Estimation of tumor cell fractions.** The tumor cell fractions harboring copy number alterations were estimated from SNP array data[60]. For a given region showing uniform copy number abnormality, the tumor content was estimated by calculating the median difference in dichotomous SNP signals at all heterozygous SNP loci within the relevant region ($\mathrm{Abn_{hetero}}$), where the median differences in intensity for dichotomous probes at all homozygous ($\mathrm{Ref_{homo}}$) and heterozygous ($\mathrm{Ref_{hetero}}$) SNPs within the largest chromosome showing normal copy numbers were used as estimates of 100% tumor content and basal noise, respectively. Thus, the tumor cell fraction (TCF) for deletions and copy-neutral LOH events was calculated by

$$\mathrm{TCF} = \frac{2\times\left(\mathrm{Abn_{hetero}} - \mathrm{Ref_{hetero}}\right)}{\left(\mathrm{Ref_{homo}} - \mathrm{Ref_{hetero}}\right)}$$

for deletions and

$$\mathrm{TCF} = \frac{\left(\mathrm{Abn_{hetero}} - \mathrm{Ref_{hetero}}\right)}{\left(\mathrm{Ref_{homo}} - \mathrm{Ref_{hetero}}\right)}$$

for copy-neutral LOH events.

Chromosomal segments showing copy number gains, which would lead to underestimation of TCF, were not used. Using TCF values, we calculated copy number–adjusted VAFs ($\mathrm{VAF_{adjusted}}$) from observed VAFs ($\mathrm{VAF_{observed}}$) as follows: $\mathrm{VAF_{adjusted}} = 2 \times \mathrm{VAF_{observed}}$ for mutations within a segment with no copy number changes, $\mathrm{VAF_{adjusted}} = \mathrm{VAF_{observed}}$ for mutations within a segment showing copy-neutral LOH and $\mathrm{VAF_{adjusted}} = \mathrm{VAF_{observed}} \times (2 - \mathrm{TCF})$ for mutations within a segment with deletion.

For mutations whose VAF was more than 0.7 VAF and that were within a segment with normal copy number, we assumed that the segment had copy-neutral LOH and that $\mathrm{VAF_{adjusted}} = \mathrm{VAF_{observed}}$. For 1p and 19q co-deletion, the tumor cell fraction was calculated as the average tumor cell fraction at 1p and 19q. Mutations in tetraploidy cases and indels of >3 bases were not analyzed because they precluded accurate estimation of VAF. For TCGA data, tumor cell fractions were estimated only for non-silent mutations of genes analyzed by targeted deep sequencing.

Finally, to adjust for the effects of varying degrees of normal contamination in different samples, the copy number–adjusted VAFs for mutations and the tumor cell fractions for arm-level deletions were divided by the maximum VAF or tumor cell fraction value to obtain the relative values within the tumor cell




doi:10.1038/ng.3273

compartment. We required that the maximum VAF value be calculated for variants supported by a depth of more than 50× to maintain accuracy.

**Bradley-Terry model.** The temporal order of mutations was estimated according to the Bradley-Terry model, in which the estimate of the temporal order was calculated together with its 95% CI, on the basis of the depth of the observed mutations and CNVs[53]. Whenever available, PCR-based deep sequencing data were used for the calculation; to avoid inappropriately narrow estimation of 95% CIs, >600× depth was rounded to 600× because the observed sequencing depths might not correctly reflect the effective number of independent reads for high depth values[61]. For CNVs, we calculated the 95% CIs from sample variance in differences for dichotomous SNP signals within the corresponding CNV region.

To apply the Bradley-Terry model, all coexisting mutations and CNVs were pitted against other mutations and CNVs. A statistically significant difference in the allelic burden was considered to exist for a given pair of coexisting mutations or deletions when the mutation or deletion with a larger VAF or tumor cell fraction was assigned to be a winner and the opposite variant was assigned to be a loser. Within the same sample, loser genes were not matched to other loser genes because these genes were considered to exist in subclones and it was difficult to determine which mutations or deletions in different subclones occurred earlier. In this analysis, some genes were categorized into several functional pathways as described above, and the Bradley-Terry model was applied to genes, gene categories and CNVs that were pitted at least five times and won at least once using the R package BradleyTerry2.

**Multiple sampling from single tumor samples.** Multi-regional sampling was performed for four tumor specimens. During operation, we collected the samples from spatially separated regions that contained apparent tumor components. The sites of sampling were recorded by the VectorVision neuronavigation system (BrainLAB). Each specimen was cut into 40- to 50-mg pieces, and DNA was extracted. Whole-exome sequence for cases where samples were collected at multiple time points or from different regions was performed using the same methods as described above except for the VAF parameters in the tumor samples, EBCall *P*-value threshold and Fisher's *P*-value threshold. To detect mutations with low VAFs, we applied VAF ≥ 0.02, EBCall *P* value < $1 \times 10^{-3}$ and Fisher's *P* value < 0.05 to mutation calling. All candidate mutations were evaluated by targeted capture sequencing or PCR-based deep sequencing using the methods described above.

**Phylogenetic trees.** To detect subpopulations, clustering analysis of mutations was performed according to the Beta Binomial emission model implemented in PyClone[62]. Mutations in repetitive regions or indels, for which VAFs were poorly estimated, were not used for the analysis. Clustering was performed using a dynamic Tree Cut procedure. When the sum of the VAFs for the second and third largest clusters of mutations was nearly equal to the VAF for the largest mutation cluster, these clusters were thought to represent 'dominant' and 'minor' subpopulations, respectively. The results of PyClone analysis are shown in **Supplementary Figure 14**. We constructed maximum-parsimony trees using the max-min branch-and-bound algorithm[63] in the MEGA6 package[64,65]. Phylogenetic trees were constructed so that the lengths of the trunks and branches were proportional to the number of mutations in between samples.


54. Nannya, Y. *et al.* A robust algorithm for copy number detection using high-density oligonucleotide single nucleotide polymorphism genotyping arrays. *Cancer Res.* **65**, 6071–6079 (2005).
55. Yamamoto, G. *et al.* Highly sensitive method for genomewide detection of allelic composition in nonpaired, primary tumor specimens by use of Affymetrix single-nucleotide-polymorphism genotyping microarrays. *Am. J. Hum. Genet.* **81**, 114–126 (2007).
56. Niida, A., Imoto, S., Shimamura, T. & Miyano, S. Statistical model-based testing to evaluate the recurrence of genomic aberrations. *Bioinformatics* **28**, i115–i120 (2012).
57. Subramanian, A. *et al.* Gene set enrichment analysis: a knowledge-based approach for interpreting genome-wide expression profiles. *Proc. Natl. Acad. Sci. USA* **102**, 15545–15550 (2005).
58. Shain, A.H. & Pollack, J.R. The spectrum of SWI/SNF mutations, ubiquitous in human cancers. *PLoS ONE* **8**, e55119 (2013).
59. Santos-Rosa, H. & Caldas, C. Chromatin modifier enzymes, the histone code and cancer. *Eur. J. Cancer* **41**, 2381–2402 (2005).
60. Katagiri, T. *et al.* Frequent loss of HLA alleles associated with copy number–neutral 6pLOH in acquired aplastic anemia. *Blood* **118**, 6601–6609 (2011).
61. Yoshida, K. *et al.* The landscape of somatic mutations in Down syndrome–related myeloid disorders. *Nat. Genet.* **45**, 1293–1299 (2013).
62. Shah, S.P. *et al.* The clonal and mutational evolution spectrum of primary triple-negative breast cancers. *Nature* **486**, 395–399 (2012).
63. Purdom, P.W. Jr., Bradford, P.G., Tamura, K. & Kumar, S. Single column discrepancy and dynamic max-mini optimizations for quickly finding the most parsimonious evolutionary trees. *Bioinformatics* **16**, 140–151 (2000).
64. Gerlinger, M. *et al.* Genomic architecture and evolution of clear cell renal cell carcinomas defined by multiregion sequencing. *Nat. Genet.* **46**, 225–233 (2014).
65. Tamura, K., Stecher, G., Peterson, D., Filipski, A. & Kumar, S. MEGA6: Molecular Evolutionary Genetics Analysis version 6.0. *Mol. Biol. Evol.* **30**, 2725–2729 (2013).